nature physics

Article

https://doi.org/10.1038/s41567-023-02360-5

Hopping frustration-induced flat band and strange metallicity in a kagome metal

Received: 11 May 2023

Accepted: 29 November 2023

Published online: 25 January 2024

Check for updates

Linda Ye[1,9], Shiang Fang[1,2], Mingu Kang[1], Josef Kaufmann[3,4], Yonghun Lee[1], Caolan John[1], Paul M. Neves[1], S. Y. Frank Zhao[1], Jonathan Denlinger[5], Chris Jozwiak[5], Aaron Bostwick[5], Eli Rotenberg[5], Efthimios Kaxiras[6,7], David C. Bell[7,8], Oleg Janson[4], Riccardo Comin[1] & Joseph G. Checkelsky[1]

The introduction of localized electronic states into a metal can alter its physical properties, for example enabling exotic metal physics including heavy fermion and strange metal behaviour. A common source of localized states in such systems are partially filled 4*f* and 5*f* shells because of the inherently compact nature of those orbitals. The interaction of electrons in these orbitals with the conduction sea is well described by the Kondo framework. However, there have also been observations of Kondo-like behaviour in 3*d* transition metal oxides and in 4*d*- and 5*d*-containing van der Waals heterostructures. This calls for a broader consideration of the physical requirements for Kondo systems. Here we show transport and thermodynamic hallmarks of heavy fermion and strange metal behaviour that arise in the kagome metal Ni_3In, wherein the source of localized states is destructive interference-induced band flattening of partially filled Ni 3*d* states. With magnetic field and pressure tuning, we also find evidence that the system is proximate to quantum criticality, extending the analogy to *f*-electron Kondo lattices. These observations highlight the role of hopping frustration in metallic systems as a potential source for strong correlations. Additionally, this suggests a lattice-driven approach to realizing correlated metals with non-trivial band topology.

Landau Fermi liquid (FL) theory is successful in describing interacting fermions in a wide variety of metals[1]. Viewed intuitively as describing systems in which the charge-carrying quasiparticles can be adiabatically connected to weakly interacting electrons in a Fermi gas[2], it explains the surprising validity of the single electron picture of metals often observed in complex, interacting materials. A celebrated case of this is conduction electrons interacting with a lattice array of localized magnetic moments (Fig. 1a)[3,4], which (via Kondo coherence) can result in a non-magnetic, renormalized FL (shown schematically in Fig. 1b) consisting of well-defined fermionic quasiparticles with hundreds of times larger effective masses (that is, heavy fermions)[5]. Another possible ground state for such a system is a metallic antiferromagnet in which FL conduction electrons mediate the interaction between local magnetic moments. It is now well established that these two FL phases

[1]Department of Physics, Massachusetts Institute of Technology, Cambridge, MA, USA. [2]Department of Physics and Astronomy, Rutgers University, Piscataway, NJ, USA. [3]Institute for Solid State Physics, TU Wien, Vienna, Austria. [4]Institute for Theoretical Solid State Physics, Leibniz IFW Dresden, Dresden, Germany. [5]Advanced Light Source, Lawrence Berkeley National Laboratory, Berkeley, CA, USA. [6]Department of Physics, Harvard University, Cambridge, MA, USA. [7]Harvard John A. Paulson School of Engineering and Applied Sciences, Harvard University, Cambridge, MA, USA. [8]Center for Nanoscale Systems, Harvard University, Cambridge, MA, USA. [9]Present address: Division of Physics, Mathematics and Astronomy, California Institute of Technology, Pasadena, CA, USA. e-mail: checkelsky@mit.edu

https://doi.org/10.1038/s41567-023-02360-5

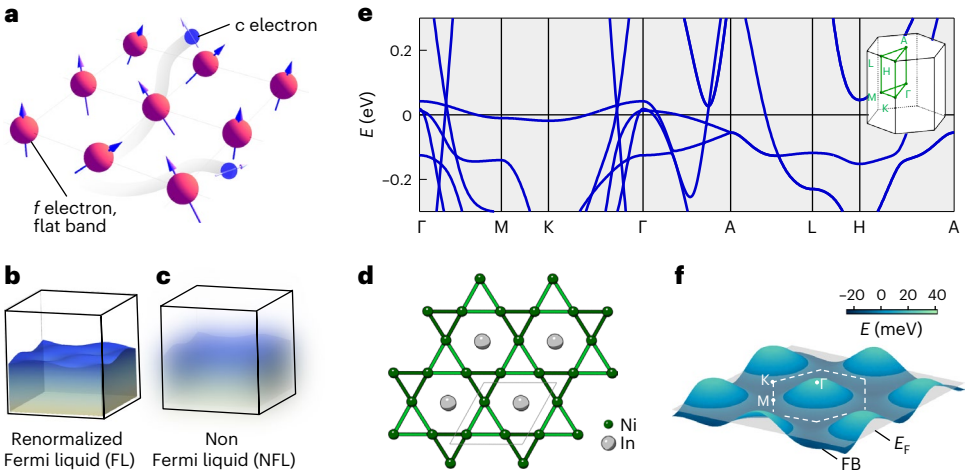

Fig. 1 | Flat band-induced emergent phases and the partial flat band in Ni_3In. a, A schematic of a Kondo lattice composed of localized electrons and conduction electrons (c electrons). The localized electrons may come from *f* electrons or flat bands. The grey traces illustrate the itinerancy of the conduction electrons. **b**,**c**, The Kondo lattice provides an avenue for renormalized (heavy) FLs (**b**) and NFL states (**c**). **d**, A top view of the Ni_3In kagome layer in the *ab* plane. Green and grey atoms represent nickel and indium, respectively. **e**, The DFT band structure of Ni_3In without spin–orbit coupling. The high-symmetry points and lines in the Brillouin zone are highlighted in the inset. **f**, A magnified view of the partial flat band (FB) within the $k_z = 0$ plane illustrated along with the Fermi level E_F.

are connected by a quantum critical point[6,7] across which FL behaviour can be disrupted. Therein, the quasiparticles no longer resemble free electrons (shown schematically in Fig. 1c), but the system remains a conductor referred to as a strange metal[8]. Such behaviour has attracted interest for both its enigmatic microscopic origin[8] and (in addition to quantum critical Kondo systems) its appearance in the normal state of high temperature superconductors[9] and, more recently, superconducting moiré heterostructures[10]. The broadening of platforms for strange metal behaviour offers an opportunity to examine its material requirements and potential insight into its underlying mechanisms.

In this Article, we study the appearance of heavy fermion and strange metal behaviour in intermetallic kagome metals. These materials have attracted considerable recent interest for their ability to host unusual topological[11–14], superconducting[15] and magnetic[11–13] phases. A striking aspect of these systems is the connection between these phases and the model expectations of the underlying trihexagonal lattice, observed as Dirac[13], van Hove[16] and flat band states[14,17]. The last among these draws connections to long-standing theoretical models for correlated electron physics based on destructive quantum interference[18]. However, the realization of ideal flat bands in kagome metals faces several challenges, including departure from the model lattice owing to hopping beyond nearest neighbour and orbital effects[14] and their stabilization at the Fermi level E_F (ref. 17). While the condition for band flatness and its isolation from other bands at the Fermi level is particularly strict for generating, for example, gapped fractional topological phases[19], we show herein that correlated metallic phases driven by a high degree of electronic degeneracy can be realized in kagome metals when narrow or partially flat bands are brought to E_F.

The transition metal intermetallic Ni_3In is a candidate for a kagome metal addressing the above criteria for a correlated metal. Crystallizing in space group $P6_3/mmc$, its basic structural unit is a breathing Ni kagome network that circumscribes In in the hexagonal void (Fig. 1d; these layers are AB stacked within a unit cell[20]). Density functional theory (DFT) calculations (Fig. 1e) indicate a partially flat band within the Γ–M–K–Γ plane at E_F. Figure 1f illustrates this dispersion, which exhibits a $k_z = 0$ bandwidth of $W_0 \approx 60$ meV. With the expected Coulomb repulsion strength of $U \approx 1$ eV as for elemental nickel[21], this implies $U \gg W_0$ for a substantial density of states even before the effects of interaction are considered. Motivated by the potential for a subsequent localized character for these electrons[21], we here explore this partial flat band and its interaction with the dispersive bands in the system in the context of a hopping interference-driven realization of the Kondo lattice (Fig. 1a).

We first examine the transport and thermodynamic properties of the metallic state of Ni_3In. The electrical resistivity in the kagome planes $\rho_{ab}(T)$ of Ni_3In at zero magnetic field is shown in Fig. 2a. Upon cooling from $T = 300$ K, $\rho_{ab}(T)$ is characterized by a broad shoulder that, below $T = 100$ K, gives way to approximately T-linear behaviour. This T-linear behaviour is a strong deviation from conventional FL behaviour ($\alpha = 2$, where α is the resistivity exponent T^α in $\rho(T)$)[22] and bears a stark contrast to several structurally related kagome metals whose $\rho(T)$ flattens out below 50 K (in which, notably, there are no partial flat bands at E_F; Supplementary Fig. S11). As shown in Fig. 2a (inset), only at $T < 1.5$ K $\equiv T_{FL}$ (T_{FL} is the temperature below which the system shows FL behaviour) a response of the form $\rho_{ab}(T) = \rho_0 + AT^2$ is recovered. The coefficient A for Ni_3In (0.25 μΩ cm K^{-2}) is orders of magnitude larger than the upper bound estimated for the isostructural Ni_3Sn (1×10^{-4} μΩ cm K^{-2}), indicating strongly enhanced electron–electron scattering in Ni_3In.

Turning to the heat capacity C_p, Fig. 2b shows C_p normalized by temperature C_pT^{-1} versus T^2 of Ni_3In. At low T, an upturn is observed, deviating from the form $\gamma + \beta T^2$ expected for a FL (where γ is the Sommerfeld coefficient and βT^2 is the phonon contribution). This becomes discernible at lower T than in electrical transport, recalling similar phenomenology reported in, for example, transition metal oxides[23,24]. Also shown is the conventional FL response for Ni_3Sn, which according to DFT exhibits a similar electronic structure apart from an overall energy shift of approximately 0.25 eV (Fig. 2b, inset). Using the acoustic phonon contribution of Ni_3Sn (Fig. 2b, dashed line), for Ni_3In we estimate $\gamma = 51.6$ mJ K^{-2} mol^{-1}, an approximately fivefold increase from 9 mJ K^{-2} mol^{-1} for Ni_3Sn. From γ, we infer a density of states $\mathcal{D}(E_F) = 44$ eV^{-1} per unit cell (u.c.) for Ni_3In, approximately three times that estimated from DFT (14 eV^{-1} u.c.$^{-1}$). In contrast, the $\mathcal{D}(E_F)$ inferred from γ (7.6 eV^{-1} u.c.$^{-1}$) is only 50% larger than that expected from DFT (4.9 eV^{-1} u.c.$^{-1}$) for Ni_3Sn. This comparison signifies considerable renormalization and correlation effects driven by the placement (before interactions) of the flat electronic states at E_F in Ni_3In. Contrasting the low-temperature A coefficient and γ additionally reveals the unusual nature of the metallic state realized in Ni_3In. This metallic state is marked by an extremely large Kadowaki–Woods ratio A/γ^2 (Fig. 2c):

https://doi.org/10.1038/s41567-023-02360-5

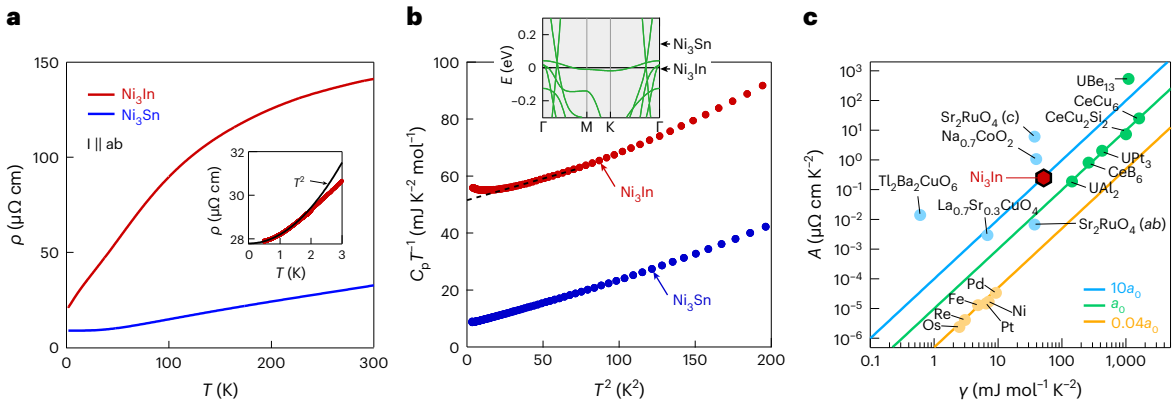

Fig. 2 | NFL behaviour and strong electron–electron scattering in Ni_3In. a, The resistivity ρ of isostructural Ni_3In (red) and Ni_3Sn (blue) as a function of temperature T in the kagome lattice plane. The inset shows ρ of Ni_3In down to 0.3 K, where FL behaviour is observed below 1.5 K. The solid black curve shows a T^2 fit to $\rho(T)$ and I is the applied current. **b**, The heat capacity normalized by temperature C_pT^{-1} of Ni_3In (red symbols) and Ni_3Sn (blue symbols) with respect to T^2. The dashed black line is an estimate of the FL C_pT^{-1} of Ni_3In with a slope taken from a linear fit to C_pT^{-1} over T^2 for Ni_3Sn below 80 K^2. The inset shows the relative electron filling of Ni_3In and Ni_3Sn in a rigid band model. **c**, The Kadowaki–Woods ratio A/γ^2 of Ni_3In in comparison with various strongly correlated electron systems in an A–γ diagram adapted from ref. 25. a_0 is a constant ($a_0 = 10$ μΩ cm $mol^2 K^2 J^{-2}$).

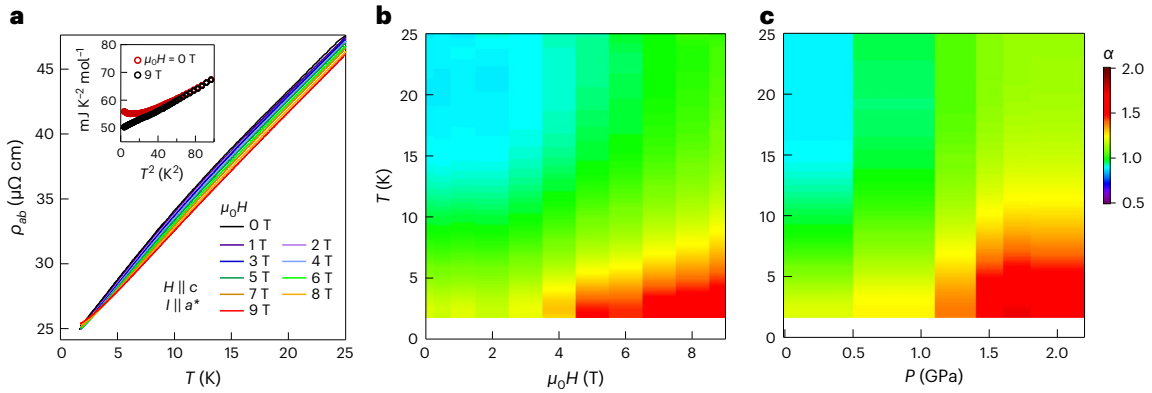

Fig. 3 | Tuning the NFL–FL crossover in Ni_3In. a, The in-plane resistivity ρ_{ab} below 25 K at various applied magnetic fields along the c axis. Here μ_0H is the applied magnetic field, and I is along a^* (perpendicular to the a axis). The inset shows the heat capacity without a magnetic field (red symbols) and with an applied field of 9 T (black symbols). **b**,**c**, The resistivity exponent α in the T–H (**b**) and T–pressure (P) (**c**) phase space. α is calculated from $d\ln(\rho - \rho_0)/d\ln T$, where ρ_0 is the extrapolated zero-temperature limit of ρ.

$A_{ab}/\gamma^2 = 91$ μΩ cm $K^2 J^{-2}$ (refs. 25,26), indicating an unconventional scattering process taking place within the kagome lattice plane. We note that the Kadowaki–Woods ratio observed in our system is three orders of magnitude larger than those of elemental transition metals and lies closer to heavy fermion metals and correlated oxides, indicating enhanced correlation in the electronic states of Ni_3In.

To shed additional light on the nature of the correlated metallic state in Ni_3In, we applied magnetic field and hydrostatic pressure as external tuning parameters to the system. Figure 3a shows high-resolution measurements of $\rho_{ab}(T, H)$ of Ni_3In. The evolution of the metallic state in Ni_3In can be seen most clearly in the map of $\alpha(T, H)$ in Fig. 3b, where the blue/green region ($\alpha = 0.9$–1) near $H = 0$ highlights a weak sublinear behaviour of ρ_{ab}. Increasing H tends to suppress the (sub)linearity and drive the system towards a FL state at low T. Quantitatively, this is reflected in a systematic decrease of A and increase of T_{FL} with H (Fig. 3b and Supplementary Figs. S14 and S15). The suppression of the zero-field non-FL (NFL) phase in field is also corroborated by C_p/T (Fig. 3a, inset). Applying a hydrostatic pressure (Fig. 3c) reveals a similar evolution of $\alpha(T, P)$, where pressure, like magnetic field, is found to suppress the NFL behaviour. We hypothesize that the observed crossover between NFL and FL states with T and magnetic field, pressure and doping (Supplementary Information Fig. S23) arises from a phase space depicted in Fig. 4a wherein fluctuations from a nearby ordered phase serve as a source of scattering tuned by the parameter δ. Such tunability is commonly observed in correlated electron systems with competing underlying energy scales[27], with the critical behaviour being described as a strange metal, often showing a T-linear behaviour over the temperature scale of associated quantum fluctuations. Notably, the overall resistivity of Ni_3In here up to room temperature (Fig. 2a) is qualitatively similar to that of the heavy fermion metal $CeCu_{5.9}Au_{0.1}$ at an antiferromagnetic quantum critical point up to 1 K (ref. 28) and to that of optimally doped $BaFe_2(As_{1-x}P_x)_2$ up to 800 K (ref. 29). The apparent common phenomenology despite the drastic difference in underlying materials and temperature scales is striking. While the multiband nature of the present system makes further quantification of the observed responses challenging, further experiments to probe potentially nearby quantum phase transitions and associated Fermi surface changes are crucial for further comparison with the broader class of strange metal systems[8].

Viewing the observed correlated metallic behaviour with the DFT electronic structure with flattened bands at E_F (Fig. 1d), we propose that the behaviour of Ni_3In can be viewed as an emergent analogue of heavy

https://doi.org/10.1038/s41567-023-02360-5

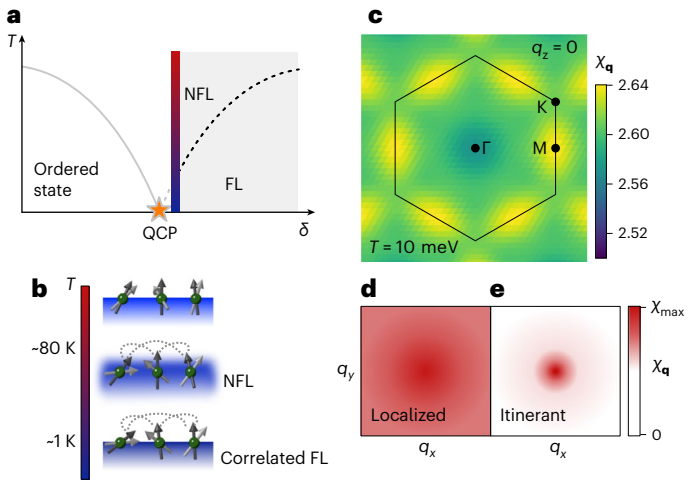

Fig. 4 | The correlated metallic state and flat band-induced magnetic fluctuations in Ni_3In. a, A hypothetical quantum critical phase diagram with external tuning parameter δ. The star indicates the quantum critical point (QCP). The thick gradient line shows the proposed location of Ni_3In at zero field and ambient pressure. The grey shaded area illustrates the parameter space traversed by magnetic field, pressure and Sn doping. The gray line indicates the hypothetical portion of the phase diagram; the dashed line marks the crossover between the FL and NFL phases. **b**, Schematics of the metallic phases realized in Ni_3In in different temperature regimes. Above 80 K, the system can be viewed as weakly correlated local moments (arrows) embedded in a conduction electron sea (blue shading). Below 80 K, a NFL phase is realized, showing a T-linear behaviour in $\rho(T)$. Below 1 K, a correlated FL phase is realized. The dotted curve indicates the correlation between the spins. **c**, The momentum-dependent susceptibility $\chi(\mathbf{q})$ of the flat band in the $q_z = 0$ plane. The colour scale of $\chi(\mathbf{q})$ is shown on the right. **d**,**e**, Schematics of $\chi(\mathbf{q})$ for localized (**d**) and itinerant (**e**) magnetic fluctuations.

fermion systems, composed of coexisting localized magnetic moments with the conduction electron sea (see the schematic in Fig. 4b). A natural source of such magnetic moments are the partial flat band states. At high T, these moments are weakly correlated, evidenced by a Curie–Weiss temperature dependence in the observed magnetic susceptibility χ as well as an onset of H suppression of fluctuations in the magnetoresistance (Supplementary Fig. S13). Below approximately 80 K, short range correlations between the moments develop, leading to a growth of $\chi(T)$ deviating from a mean-field Curie-Weiss form, and intense scattering of the conduction electrons including an approximate T-linear (strange metal) behaviour for $\rho_{ab}(T)$, defining a NFL regime in Fig. 4a,b. Finally, for $T < 1$ K, a heavily renormalized metallic state appears, marked by strongly enhanced scattering in the kagome plane.

Whereas the conventional starting point for modelling of heavy fermion systems is a localized moment interacting with a conduction electron sea, in the present case, we hypothesize that both of these constituent elements arise from band features. In the following, we discuss the potential origin of the former from a band theoretical perspective. The flat electronic states near E_F are found to be composed of d_{xz} orbitals in locally rotated coordinates. Using an effective band model aimed at capturing these states, we performed local χ_{loc} and momentum-resolved magnetic susceptibility $\chi(\mathbf{q})$ calculations (Supplementary Section SIII). A pronounced Curie–Weiss-like increase of χ_{loc} with lowering T in the absence of correlation indicates a pre-formation of local moments[21] (Supplementary Fig. S7). Additionally, $\chi(\mathbf{q})$ exhibits negligible momentum dependence in the kagome plane (Fig. 4c). The presence of an extended 'hot region' across the kagome plane suggests that the magnetic instability of the partially filled flat band is of localized nature (Fig. 4d), distinct from prototypical itinerant magnetic orders driven by 'hot spots' in momentum space (Fig. 4e)[30].

The above analysis supports the formation of local moments in the system when correlation is further introduced[21]. Upon the formation of local moments, the low-energy physics is then dominated by how the array of local moments interact with the conduction electrons in the system, akin to heavy fermion and NFL behaviours observed in Kondo lattice systems[22]. We note that the observed pressure and field-driven crossover between NFL and FL is consistent with this picture: in the context of the Doniach phase diagram[4], pressure is expected to favour a screened heavy fermion liquid phase by increasing J, while magnetic field is found to favour a FL phase as a result of suppression of magnetic fluctuations in a variety of Kondo lattice quantum critical systems[28,31]. The present system therefore establishes a distinct route to heavy fermion and associated quantum criticality from a pure band origin, potentially connecting to recent theoretical proposals for flat-band-driven Kondo behaviour with elevated energy scales[32].

Tuning Ni_3In across a potential quantum phase transition into an ordered state as illustrated in the hypothetical phase diagram in Fig. 4a should help shed further light on the interaction between the conduction electron and the flat band electrons and put further constraints on theoretical models that can capture the low-energy physics, particularly the NFL/strange metal behaviour. Although it is found that neither magnetic field nor pressure can induce an ordered phase, future experimental exploration of the phase space spanned by additional non-thermal tuning parameters such as uniaxial stress, negative chemical pressure or carrier doping are important to clarify the nature of potentially nearby magnetic and electronic instabilities. The breathing kagome lattice in Ni_3In itself in the context of antiferromagnetic interaction may lead to strong geometric frustration and emergent spin excitations relevant to understanding the present strange metal behaviour[33,34]. We note that Ni_3In also hosts a mirror-protected nodal ring near E_F (Fig. 1d and Supplementary Fig. S2), providing a unique platform where topological electronic features may interact with a NFL state at E_F. It is also of considerable future theoretical interest to compare the observed NFL behaviours in the present system with structurally related CoSn—which hosts flat bands with different dimensionality and/or orbital characters compared with the present system—as the Fermi level is tuned through the flat bands therein[14,35].

The key design aspect here to realize the unusual metallic states in Ni_3In lies in the frustration of hopping of the states at E_F from cooperative destructive interference between lattice and orbital degrees of freedom. Our approach exemplifies an increased role of designing correlated systems from a non-interacting starting point, and in the meantime leverages the broad notion of using 3d electrons to increase interaction effects[36]. This suggests potential new insights into the behaviour of previously reported d-electron heavy fermion systems that arise from frustrated networks (for example, the V pyrochlore-containing system LiV_2O_4[37]) and van der Waals heterostructures[38,39], and more broadly, a design paradigm for realizing correlated topological states[40]. Additionally, despite this marked departure from the f-electron design paradigm[5], the resulting transport and quantum critical phenomenology is strikingly similar. Common among these systems is the realization of flattened electronic dispersion near the Fermi level, raising the possibility that the unifying driver for heavy fermion and strange metal behaviour therein is 'flat band' metallic states[32,41,42]. Such a broadened range of systems represents a vastly differentiated material landscape for examining theories of strongly correlated gapless phases.

Online content

Any methods, additional references, Nature Portfolio reporting summaries, source data, extended data, supplementary information, acknowledgements, peer review information; details of author contributions and competing interests; and statements of data and code availability are available at https://doi.org/10.1038/s41567-023-02360-5.

References

1. Baym, G. & Pethick, C. *Landau Fermi-Liquid Theory: Concepts and Applications* (Wiley, 2008).
2. Anderson, P. W. *Basic Notions of Condensed Matter Physics* (CRC Press, 2018).
3. Kondo, J. Resistance Minimum in Dilute Magnetic Alloys. *Prog. Theor. Phys.* **32**, 37 (1964).
4. Doniach, S. The Kondo lattice and weak antiferromagnetism. *Phys. B+C* **91**, 231 (1977).
5. Coleman, P. in *Handbook of Magnetism and Advanced Magnetic Materials* (eds Kronmuller, H. & Parkin, S.) pp 95–148 (Wiley, 2007).
6. Gegenwart, P., Si, Q. & Steglich, F. Quantum criticality in heavy-fermion metals. *Nat. Phys.* **4**, 186–197 (2008).
7. Si, Q. & Steglich, F. Heavy fermions and quantum phase transitions. *Science* **329**, 1161 (2010).
8. Phillips, P. W., Hussey, N. E. & Abbamonte, P. Stranger than metals. *Science* **377**, eabh4273 (2022).
9. Proust, C. & Taillefer, L. The remarkable underlying ground states of cuprate superconductors. *Annu. Rev. Condens. Matter Phys.* **10**, 409 (2019).
10. Jaoui, A. et al. Quantum critical behaviour in magic-angle twisted bilayer graphene. *Nat. Phys.* **18**, 633–638 (2022).
11. Nayak, A. K. et al. Large anomalous Hall effect driven by a nonvanishing Berry curvature in the noncolinear antiferromagnet Mn_3Ge. *Sci. Adv.* **2**, e1501870 (2016).
12. Nakatsuji, S., Kiyohara, N. & Higo, T. Large anomalous Hall effect in a non-collinear antiferromagnet at room temperature. *Nature* **527**, 212–215 (2015).
13. Ye, L. et al. Massive Dirac fermions in a ferromagnetic kagome metal. *Nature* **555**, 638–642 (2018).
14. Kang, M. et al. Topological flat bands in frustrated kagome lattice CoSn. *Nat. Commun.* **11**, 4004 (2020).
15. Ortiz, B. R. et al. CsV_3Sb_5: a z_2 topological kagome metal with a superconducting ground state. *Phys. Rev. Lett.* **125**, 247002 (2020).
16. Kang, M. et al. Twofold van Hove singularity and origin of charge order in topological kagome superconductor CsV_3Sb_5. *Nat. Phys.* **18**, 301–308 (2022).
17. Kang, M. et al. Dirac fermions and flat bands in the ideal kagome metal FeSn. *Nat. Mater.* **19**, 163–169 (2020).
18. Bergman, D. L., Wu, C. & Balents, L. Band touching from real-space topology in frustrated hopping models. *Phys. Rev. B* **78**, 125104 (2008).
19. Tang, E., Mei, J.-W. & Wen, X.-G. High-temperature fractional quantum Hall states. *Phys. Rev. Lett.* **106**, 236802 (2011).
20. Baranova, R. An electron diffraction study of the Ni–In system. *Sov. Phys. Crystallogr.* **10**, 523–528 (1966).
21. Hausoel, A. et al. Local magnetic moments in iron and nickel at ambient and Earth's core conditions. *Nat. Commun.* **8**, 16062 (2017).
22. Stewart, G. Non-Fermi-liquid behavior in *d*- and *f*-electron metals. *Rev. Mod. Phys.* **73**, 797 (2001).
23. Daou, R. et al. Linear temperature dependence of resistivity and change in the fermi surface at the pseudogap critical point of a high-t_c superconductor. *Nat. Phys.* **5**, 31–34 (2009).
24. Michon, B. et al. Thermodynamic signatures of quantum criticality in cuprate superconductors. *Nature* **567**, 218–222 (2019).
25. Li, S. et al. Giant electron–electron scattering in the Fermi-liquid state of $Na_{0.7}CoO_2$. *Phys. Rev. Lett.* **93**, 056401 (2004).
26. Jacko, A., Fjærestad, J. & Powell, B. A unified explanation of the Kadowaki–Woods ratio in strongly correlated metals. *Nat. Phys.* **5**, 422–425 (2009).
27. Dagotto, E. Complexity in strongly correlated electronic systems. *Science* **309**, 257 (2005).
28. Löhneysen, H. V. et al. Non-Fermi-liquid behavior in a heavy-fermion alloy at a magnetic instability. *Phys. Rev. Lett.* **72**, 3262 (1994).
29. Hu, D. et al. ω/T scaling and magnetic quantum criticality in $BaFe_2(As_{0.7}P_{0.3})_2$. Preprint at https://arxiv.org/abs/1812.11902 (2018).
30. Moriya, T. Recent progress in the theory of itinerant electron magnetism. *J. Magn. Magn. Mater.* **14**, 1 (1979).
31. Coleman, P. & Nevidomskyy, A. H. Frustration and the Kondo effect in heavy fermion materials. *J. Low. Temp. Phys.* **161**, 182 (2010).
32. Chen, L. et al. Emergent flat band and topological Kondo semimetal driven by orbital-selective correlations. Preprint at https://arxiv.org/abs/2212.08017 (2022).
33. Motrunich, O. I. Variational study of triangular lattice spin-1/2 model with ring exchanges and spin liquid state in κ-$(ET)_2Cu_2(CN)_3$. *Phys. Rev. B* **72**, 045105 (2005).
34. Zhao, H. et al. Quantum-critical phase from frustrated magnetism in a strongly correlated metal. *Nat. Phys.* **15**, 1261–1266 (2019).
35. Sales, B. C. et al. Chemical control of magnetism in the kagome metal $CoSn_{1-x}In_x$: magnetic order from nonmagnetic substitutions. *Chem. Mater.* **34**, 7069 (2022).
36. Smith, J. & Kmetko, E. Magnetism or bonding: a nearly periodic table of transition elements. *J. Less Common Met.* **90**, 83 (1983).
37. Kondo, S. et al. LiV_2O_4: a heavy fermion transition metal oxide. *Phys. Rev. Lett.* **78**, 3729 (1997).
38. Vaňo, V. et al. Artificial heavy fermions in a van der Waals heterostructure. *Nature* **599**, 582–586 (2021).
39. Zhao, W. et al. Gate-tunable heavy fermions in a moiré Kondo lattice. *Nature* **616**, 61–65 (2023).
40. Chen, L. et al. Topological semimetal driven by strong correlations and crystalline symmetry. *Nat. Phys.* **18**, 1341–1346 (2022).
41. Song, Z.-D. & Bernevig, B. A. Magic-angle twisted bilayer graphene as a topological heavy fermion problem. *Phys. Rev. Lett.* **129**, 047601 (2022).
42. Regnault, N. et al. Catalogue of flat-band stoichiometric materials. *Nature* **603**, 824–828 (2022).

Methods

Materials synthesis

Single crystals of Ni_3In were synthesized via an I_2-catalysed reaction. The starting materials of Ni and In powders in 3:1 molar ratio were mixed with I_2 pieces and sealed in an evacuated quartz tube. The quartz tube was heated up to 800 °C and kept for more than 2 weeks. Hexagonal prism-shaped crystals (with typical lateral size of 300–500 μm) can be obtained and are found to be stable in air. Single crystals of Ni_3Sn were synthesized via chemical vapour transport. Ni powder and Sn pieces at 3:1 molar ratio were loaded into an evacuated quartz tube with the addition of 5 mg cm^{-3} I_2. The growth took place at a temperature gradient from 850 to 700 °C for 2 weeks, and the primary morphology of the crystals was needle like. The phase of the crystals was confirmed by X-ray diffraction analysis. Polycrystals of $Ni_3In_{1-x}Sn_x$ were synthesized by mixing the stoichiometric powder and kept in evacuated quartz tubes at 800 °C for 3–5 days. The product was ground to powder, and the above process was repeated multiple times to improve homogeneity. Polycrystalline samples for heat capacity measurements were pelletized and sintered at 800 °C for 3–5 days. Scanning electron microscopy images of single crystals were taken in a FEI Helios Nanolab 600 dual beam microscope.

Physical properties measurements

Electrical transport measurements were performed on single crystals and polycrystals with the standard five-probe method in a commercial cryostat and also at the National High Magnetic Field Laboratory (NHMFL) d.c. field facility. We used a focused ion beam to structure a thin piece of crystal (~5 μm thick) for transport measurements. The focused ion beam fabrication was performed with a FEI Helios Nanolab 600 dual beam microscope with a Ga-ion beam flux of 21 nA at a magnification of 350. Resistivity measurements under hydrostatic pressure were performed in an HPC-33 piston-type pressure cell (ElectroLab Corp.) with Daphne7373 as the pressure transmitting medium. Heat capacity measurements were performed on sintered polycrystals using the two-relaxation-time method. In-house magnetic susceptibility measurements were performed in a vibrating sample magnetometer with a Quantum Design Magnetic Property Measurement System (MPMS3). Magnetization measurements up to 60 T were performed at the NHMFL pulsed field facility at the Los Alamos National Laboratory.

Scanning transmission electron microscopy

Scanning transmission electron microscopy experiments were conducted on a JEOL ARM 200CFG probe corrected microscope at an accelerating voltage of 200 kV. Ni_3In samples were prepared by a Helios focused ion beam (Thermo Electron) operated at an acceleration voltage of 30 kV for the gallium beam lift-out, followed by a 1 keV final argon polish with a (Fischione) Nanomill for 15 min.

Angle-resolved photoemission spectroscopy

Angle-resolved photoemission spectroscopy experiments (ARPES) were performed at Beamline 7.0.2 (MAESTRO) of the Advanced Light Source. The experiments were conducted at the micro-ARPES endstation equipped with a R4000 hemispherical electron analyser (Scienta Omicron). Ni_3In samples were not cleavable by standard post-cleaving procedure. We thus prepared the surface of Ni_3In by ex situ fine polishing followed by in situ Ar^+-ion sputtering and annealing at 700 °C. Recovery of the Ni_3In surface structure after the sputter–annealing cycles was confirmed by in situ low-energy electron diffraction feedback. The atomically flat surface of Ni_3Sn was prepared by standard in situ low-temperature cleaving. ARPES measurements were conducted at liquid nitrogen temperature (~80 K) and under ultrahigh vacuum better than 4×10^{-11} torr. Photon energy dependence was investigated over a wide energy range from 70 to 230 eV to identify high-symmetry positions along the k_z momentum space directions. The high-symmetry points (Γ and Z) and periodicity along k_z were well reproduced through the nearly-free-electron final state model with inner potential of 10 eV. All spectra were collected with *p*-polarized photons. The energy and momentum resolutions were below 20 meV and 0.01 $Å^{-1}$, respectively.

First-principles electronic structure calculations

Ab initio DFT calculations were performed by using the Vienna Ab Initio Simulation Package (VASP)[43,44]. The pseudo-potential formalism was based on the projector augmented wave method[45] with exchange–correlation energy as parametrized by Perdew, Burke and Ernzerhof (PBE)[46], a functional of the generalized gradient approximation type. The DFT calculations for the bulk Ni_3In crystal were converged with an energy cut-off of 360 eV for the plane wave basis and a $13 \times 13 \times 11$ Monkhorst–Pack grid sampling in reciprocal space. To analyse the DFT electronic structure, we employed the Wannier90 code[47,48] to construct the Wannier tight-binding Hamiltonian[49], using the localized Wannier basis projected from Ni 3*d* and 4*s* and In 5*s* states. The further simplified effective six-band model projected from the locally rotated d_{xz} orbitals was also derived similarly.

To construct an effective model based on molecular rather than atomic orbitals, we additionally carried out DFT calculations using the full-potential local-orbital code FPLO[50] (version 18). Its built-in module[51] allows the user to construct Wannier projections for molecular-like states comprising several atomic orbitals. Since the generalized gradient approximation orbital-resolved density of states revealed the dominance of Ni d_{xy} and d_{xz} contributions in the vicinity of the Fermi level, we restricted ourselves to these atomic orbitals. Molecular orbitals were constructed by combining the respective orbitals of three Ni atoms forming a triangle on the kagome lattice. In this way, we obtained an effective model with two sites per cell and two orbitals per site, giving rise to four bands. To cross-check results for magnetic susceptibilities calculated using different models, we also performed an automatic wannierization, which yields a model describing all valence states (excluding core and semi-core states).

With the effective model, we evaluated the local magnetic susceptibility χ^0_{loc}, defined as

$$\chi^0_{\mathrm{loc}}(\omega = 0) = -\frac{2\mu_{\mathrm{B}}^2}{\beta} \sum_{ij} \sum_{\omega_n} G^{0,\mathrm{loc}}_{ij}(\omega_n) G^{0,\mathrm{loc}}_{ji}(\omega_n), \quad (1)$$

with the Bohr magneton μ_{B} and Matsubara frequency ω_n and $G^{0,\mathrm{loc}}_{ij}(\omega_n) = \frac{1}{N_{\mathbf{k}}} \sum_{\mathbf{k}} G^0_{ij}(\mathbf{k}, \omega_n)$. The Curie–Weiss-like temperature dependence χ^0_{loc} for the Ni_3In effective model can be contrasted with a simple metal, modelled by a single-band three-dimensional cubic lattice with an energy dispersion of $E = (\cos(k_x) + \cos(k_y)) + \cos(k_z))/3$. We calculated χ^0_{loc} using a $24 \times 24 \times 24$ momentum sampling grid with a bandwidth of 2 eV and chemical potential at $E = 0.5$ eV,

Data availability

The datasets for the main text are available in the Supplementary Information. All other data are available from the corresponding author on reasonable request. Source data are provided with this paper.

Code availability

The codes used to support the findings in this study are available from the corresponding author on reasonable request.

References

43. Kresse, G. & Furthmüller, J. Efficient iterative schemes for ab initio total-energy calculations using a plane-wave basis set. *Phys. Rev. B* **54**, 11169 (1996).
44. Kresse, G. & Furthmüller, J. Efficiency of ab-initio total energy calculations for metals and semiconductors using a plane-wave basis set. *Comput. Mater. Sci.* **6**, 15 (1996).

45. Blöchl, P. E. Projector augmented-wave method. *Phys. Rev. B* **50**, 17953 (1994).
46. Perdew, J. P., Burke, K. & Ernzerhof, M. Generalized gradient approximation made simple. *Phys. Rev. Lett.* **77**, 3865 (1996).
47. Mostofi, A. A. et al. wannier90: a tool for obtaining maximally-localised Wannier functions. *Comput. Phys. Commun.* **178**, 685 (2008).
48. Mostofi, A. A. et al. An updated version of wannier90: a tool for obtaining maximally-localised Wannier functions. *Comput. Phys. Commun.* **185**, 2309 (2014).
49. Marzari, N., Mostofi, A. A., Yates, J. R., Souza, I. & Vanderbilt, D. Maximally localized Wannier functions: theory and applications. *Rev. Mod. Phys.* **84**, 1419 (2012).
50. Koepernik, K. & Eschrig, H. Full-potential nonorthogonal local-orbital minimum-basis band-structure scheme. *Phys. Rev. B* **59**, 1743 (1999).
51. Eschrig, H. & Koepernik, K. Tight-binding models for the iron-based superconductors. *Phys. Rev. B* **80**, 104503 (2009).

Acknowledgements

We appreciate fruitful discussions with T. Senthil, B. J. Yang, L. Zou, Y. Zhang, K. Haule, J.-S. You, J. van den Brink, O. I. Motrunich, S. Bühler-Paschen, Q. Si, C. Varma and M. Kriener. L.Y. acknowledges assistance from M.K. Chan for pulsed field magnetization measurements. D.C.B. acknowledges help from A. Akey for TEM sample preparation. This research is funded in part by the Gordon and Betty Moore Foundation EPiQS Initiative, through grants GBMF3848 and GBMF9070 to J.G.C. (material synthesis), NSF grant DMR-1554891 (material design), ARO grant no. W911NF-16-1-0034 (technique development) and the Air Force Office of Scientific Research under award FA9550-22-1-0432 (advanced material analysis). L.Y., M.K. and E.K. acknowledge support by the STC Center for Integrated Quantum Materials, NSF grant number DMR-1231319. L.Y. acknowledges the Heising-Simons Physics Research Fellow Program and the Tsinghua Education Foundation. S.F. is partially supported by a Rutgers Center for Material Theory Distinguished Postdoctoral Fellowship. M.K. acknowledges support from the Samsung Scholarship from the Samsung Foundation of Culture. R.C. acknowledges support from the Alfred P. Sloan Foundation. O.J. was supported by the Leibniz Association through the Leibniz Competition. A portion of this work was performed at the National High Magnetic Field Laboratory, which is supported by National Science Foundation cooperative agreement no. DMR-1644779, the State of Florida and the Department of Energy (DOE). Pulsed magnetic field measurements at Los Alamos National Laboratory were supported by the US Department of Energy BES Science at 100T grant. This research used the resources of the Advanced Light Source, a US DOE Office of Science User Facility under contract no. DE-AC02-05CH11231. The computations in this paper were run on the ITF/IFW computer clusters (Dresden, Germany) and the FASRC Cannon cluster supported by the FAS Division of Science Research Computing Group at Harvard University. We thank U. Nitzsche for technical assistance in maintaining computing resources at IFW Dresden. This work was performed in part at the Aspen Center for Physics, which is supported by National Science Foundation grant PHY-1607611.

Author contributions

L.Y. and J.G.C. designed the study. L.Y. synthesized and characterized the single crystalline and polycrystalline materials, and performed and analysed the physical property measurements, with C.J. (hydrostatic pressure measurements), P.M.N. (rotation measurements) and S.Y.F.Z. (low temperature measurements). S.F., J.K., O.J. and E.K. performed the first principles analysis. M.K., Y.L. and R.C. performed the photoemission experiments and analysis with the assistance of J.D., C.J., A.B. and E.R. J.D. guided the process of sample surface preparation. D.C.B. performed the transmission electron microscopy measurements. L.Y. and J.G.C. wrote the manuscript with input from all the other authors.

Competing interests

The authors declare no competing interests.

Additional information

Supplementary information The online version contains supplementary material available at https://doi.org/10.1038/s41567-023-02360-5.

Correspondence and requests for materials should be addressed to Joseph G. Checkelsky.

Peer review information *Nature Physics* thanks William Meier and the other, anonymous, reviewers for their contribution to the peer review of this work.